View metadata, citation and similar papers at core.ac.uk

brought to you by CORE

provided by Explore Bristol Research

Conti, S., Vila, B., Sellés, A. G., Galobart, À., Benton, M. J., & Prieto-Márquez, A. (2020). The oldest lambeosaurine dinosaur from Europe: Insights into the arrival of Tsintaosaurini. *Cretaceous Research*, *107*, [104286]. https://doi.org/10.1016/j.cretres.2019.104286

Peer reviewed version

License (if available):
CC BY-NC-ND

Link to published version (if available):
10.1016/j.cretres.2019.104286

Link to publication record in Explore Bristol Research
PDF-document

This is the author accepted manuscript (AAM). The final published version (version of record) is available online via Elsevier at https://www.sciencedirect.com/science/article/pii/S0195667119301879#:~:text=Hollow%2Dcrested%20lambeosaurine%20hadrosaurids%20represent,distribution%20during%20the%20Late%20Cretaceous . Please refer to any applicable terms of use of the publisher.

University of Bristol - Explore Bristol Research

General rights

This document is made available in accordance with publisher policies. Please cite only the published version using the reference above. Full terms of use are available:
http://www.bristol.ac.uk/red/research-policy/pure/user-guides/ebr-terms/

The oldest lambeosaurine dinosaur from Europe: insights into the arrival of Tsintaosaurini

Simone Conti[a], Bernat Vila[b,c,d], Albert G. Sellés[b,c], Àngel Galobart[b,c], Michael J. Benton[a], Albert Prieto-Márquez[a,b*],

[a] School of Earth Sciences, University of Bristol, Life Sciences Building, 24 Tyndall Avenue, Bristol BS8 1TQ, United Kingdom

[b] Institut Català de Paleontologia Miquel Crusafont, Universitat Autònoma de Barcelona, Carrer de l'Escola Industrial 23, 08201 Sabadell, Barcelona, Spain

[c] Museu de la Conca Dellà-Parc Cretaci, Carrer del Museum 4, 25650 Isona, Lleida, Spain

[d] Departament de Geologia, Facultat de Ciències, Universitat Autònoma de Barcelona, Carrer de l'Eix central, 08193, Cerdanyola del Vallès, Barcelona, Spain

Corresponding author. E-mail: redshore@gmail.com

Abstract

The hollow-crested lambeosaurine hadrosaurids represent one of the latest and most rapid radiations of ornithischian dinosaurs, attaining a nearly global distribution during the Late Cretaceous. Although their presence in Europe is well documented, there are questions about the origin and timing of their arrival in this continent. The analysis of old and newfound lambeosaurine specimens from the Els Nerets locality (eastern Tremp Syncline, northeastern Spain) have shown that the ornithopod dinosaurs from this classic site belong to Lambeosaurinae. Recent chronostratigraphic data places the locality in the lower Maastrichtian, implying that the Els Nerets lambeosaurine is the first occurrence of the clade in Europe. The Els Nerets lambeosaurine exhibits some noticeable pelvic features only shared with the Asian taxon *Tsintaosaurus spinorhinus* and thus we hypothesize a close taxonomic affinity between the lambeosaurine from Els Nerets and the Eurasian Tsintaosaurini. Members of this tribe would have dispersed into the Ibero-Armorican Domain not later than the early Maastrichtian, coexisting with endemic dinosaurian groups for some time.

Keywords: anatomy, phylogeny, biogeography, Cretaceous, Hadrosauridae, Lambeosaurinae

1. Introduction

European Late Cretaceous dinosaurs have been described from Austria, Belgium, Germany, Hungary, Italy, Portugal, Slovenia, Sweden, the Netherlands (Buffetaut, 2009; Dalla Vecchia, 2014; Csiki-Sava et al., 2015), and more prominently from the Haţeg Basin of Romania (Benton et al., 2010; Csiki-Sava et al., 2015), Spain (Puértolas-Pascual et al., 2018; Canudo et al., 2016; Cruzado-Caballero et al., 2010, 2013; Company et al., 2015; Pereda-Suberbiola et al., 2009), and southern France (Csiki-Sava et al., 2015; Dalla Vecchia, 2014; Dalla Vecchia et al., 2014; Prieto-Márquez et al., 2013). Among the various clades recorded in this region of the Globe, lambeosaurine hadrosauroids are probably the most commonly found (Pereda-Suberbiola et al., 2009; Cruzado-Caballero et al., 2010; Prieto-Márquez et al., 2013; 2019; Dalla Vecchia et al., 2014; Fondevilla et al., 2018). Specifically, they are uniquely found in the Ibero-Armorican domain, the largest island of the Late Cretaceous European archipelago. In this region their stratigraphic distribution is restricted to the Maastrichtian, while worldwide their fossils range from Santonian to the upper Maastrichtian strata in Asia and North America (Prieto-Márquez, 2010). European hadrosaurids are so far represented by five species, four of them from the late Maastrichtian: *Pararhabdodon isonensis* Casanovas-Cladellas et al., 1993; *Arenysaurus ardevoli* Pereda-Superbiola et al., 2009; *Blasisaurus canudoi* Cruzado-Caballero et al., 2010, *Canardia garonnensis* Prieto-Márquez et al., 2013 and one from the early Maastrichtian *Adynomosaurus arcanus* Prieto-Márquez et al., 2019.

To date, the appearance of lambeosaurine dinosaurs in the Ibero-Armorican island, and therefore in the European archipelago is dated “sometime during the Maastrichtian” (Prieto-Márquez et al., 2013, p. 1). However, tsintaosaurin osteological data was lacking from lower Maastrichtian sites. The presence of hadrosaurids at that time had a significant impact on the reorganization of vertebrate faunas during the latest Cretaceous of southwestern Europe,

coinciding with the final stages of the faunal turnover interval (Vila et al., 2016; Fondevilla et al., 2019).

In the context of this temporal and palaeobiogeographic scenario, we revisited the lower Maastrichtian locality of Els Nerets, in the eastern Tremp syncline (NE Spain). We review the previously published material of hadrosaurids and describe new fossils of this clade in order to reassess a possible first occurrence of lambeosaurine fossils in Europe and their arrival from Asia. Further, recent chronostratigraphic calibrations in the region indicate that the site is important as the oldest in western Europe preserving unequivocal evidence of hadrosaurids, as part of a diverse and transitional ecosystem composed ofy plants and palynomorphs (Torices et al., 2012), fishes (Blanco et al., 2017), turtles, crocodylians (Buscalioni et al., 1986, Blanco, 2017), as well as theropod, ankylosaurian, and sauropod dinosaurs (Casanovas et al., 1987; Riera et al., 2009; Dalla Vecchia et al., 2014).

Institutional abbreviations—AEMH, Amur Natural History Museum, Blagoveschensk, Russia; **CMN**, Canadian Museum of Nature, Ottawa, Canada; **FMNH**, The Field Museum, Chicago, U.S.A; **IPS**, Institut Català de Paleontologia Miquel Crusafont, Sabadell, Spain; **IVPP**, Institute of Vertebrate Paleontology and Paleoanthropology, Beijing, China; **LACM**, Natural History Museum of Los Angeles County, Los Angeles, U.S.A; **MCD**, Museu de la Conca Dellà, Isona, Spain; **MDE**, Musée des Dinosaures d'Espéranza, France; **MOR**, Museum of the Rockies, Bozeman, U.S.A; **MPZ**, Museo Paleontológico de la Universidad de Zaragoza, Zaragoza, Spain.

2. Els Nerets locality

2.1 Geological Setting

94 The locality of Els Nerets is located 500 m north of Vilamitjana village, near the town
95 of Tremp (Lleida province, northwestern Catalonia; Fig. 1). The locality exposes deposits of
96 La Posa Formation of the Tremp Group (Fig. 2), in the Tremp syncline, one of the four
97 Cretaceous basins that occur in the southern Pyrenees (Fig. 1). The Maastrichtian to Thanetian
98 materials of the Tremp Group (Mey et al., 1968) are widely exposed in the southern flank of
99 the Pyrenees, overlying or interfingering to the east with the Arén Sandstone Formation,
100 recording a regressive trend that started at the Campanian-Maastrichtian boundary (Rosell et
101 al., 2001). The Tremp Group has been divided into four units, from the base to the top as
102 follows: 1) La Posa Formation (Cuevas, 1992), also referred to as "Grey Unit" or "Grey
103 Garumnian" (Rosell et al., 2001), consisting of alternations of grey marlstones and
104 sandstones, deposited in lagoon settings with mudflats, freshwater lakes and marshes; 2)
105 Conques Formation (Cuevas, 1992), also referred to as "Lower Red Unit", consisting of
106 reddish and brownish mudstones deposited in floodplains and fluvial deposits with tidal
107 influence; 3) Talarn Formation (Cuevas, 1992), also referred to as "Vallcebre limestones",
108 consisting of sandstones and conglomerates deposited in lacustrine environments, and 4)
109 Suterranya Formation (Cuevas, 1992), also referred to as "Upper Red Unit", an alternation of
110 limestones and mudstones deposited in a fluvial-alluvial environment. Stratigraphic data
111 (biostratigraphy, magnetostratigraphy and correlation with other units) indicate a
112 Maastrichtian age for the Cretaceous portion of the Tremp Group (La Posa and Conques
113 Formations) in the Tremp syncline (Diez-Canseco et al., 2014; Fondevilla et al., 2017; Riera
114 et al., 2009, Villalba-Breva and Martin-Closas, 2013).
115 The site of Els Nerets is lateral to the Vicari section, noted by Torices et al. (2012).
116 There the authors identified three stratigraphic units through the 42 m stratigraphic section:
117 the Arén Sandstone Formation is present as the lowermost and the uppermost units, composed
118 of clean, mature, mixed carbonate-cemented shoreface-to-near-shore arenite with rudists and

grey offshore marls with inoceramids; the top of this bed is composed of middle-grained hybrid arenite modified by reddish-ochre mottling and iron crusts containing abundant dinosaur eggshells and isolated bones; the uppermost unit is formed from marine calcarenites and sandy limestones showing wackestone-packestone texture and wavy cross stratification. The two Arén Sandstone Formation units are separated by La Posa Formation strata belonging to the Tremp Group, which changes notably from East to West, forming a local furrow or lens-shaped geometry with a maximum thickness around 40 m. The lower 21 m thick portion mostly consists of grey mudstones. In its middle part, the mudstone evolves into a grey sandstone showing a well-developed paleosol at the top. Approximately one metre above the paleosol, a one metre thick marly limestone occurs. The fossils herein were found at the base of this marly limestone bed. The upper 15 m thick portion of the Tremp Group is composed of ochre and purple mudstones. Based on lithological and palynological content, three transgressive-regressive episodes have been identified (Torices et al., 2012), with the Arén Sandstone Formation representing fully marine deposition, whereas the Tremp Group beds suggest a lagoonal environment that evolved to more drained conditions in its upper portion. The dominance of planktonic marine organisms near the top of the grey unit indicates a dramatic transgression that was not recorded in the lithology (Torices et al., 2012). Magnetostratigraphically, Els Nerets locality is correlated with the magnetochrone C31r and biostratigraphic and lithostratigraphic correlations indicate a lower Maastrichtian age for Els Nerets, ca. 70 Ma (Fondevilla et al., 2017; 2019).

2.2 Faunal content

The Els Nerets locality was first discovered and excavated in 1984 (Casanovas et al., 1987; Buscalioni et al., 1986), a second research phase started in 2003 with a series of prospections and excavations (Gaete et al., 2003) and later with systematic excavations from

2013 to 2018. During these years dozens of specimens were collected, revealing a diverse fauna. The locality has yielded plant remains, teeth and scales of fishes, bones of turtles, bones and teeth of crocodiles, teeth of indeterminate theropod, teeth and bones of titanosaur sauropods, osteoderms of indeterminate ankylosaurians and bones and tracks of hadrosaurids. The earliest finding of hadrosaurid bones at this locality were formerly referred to the genus "Orthomerus" (Casanovas-Cladellas et al., 1985), currently a *nomen nudum* (Brinkmann, 1988; Horner et al., 2004).

The bones are found at the base of a one metre thick marly limestone bed of the lower Maastrichtian La Posa Formation. The skeletal elements recovered in the 2013–2018 fieldwork seasons were found disarticulated and their orientation was given by the angle between the north and the major axis of the bones. After plotting the bones in a 180° rose diagram in order to determine the main direction of flow that transported the fossil elements, 29 bones revealed a mean orientation of 70.65° to the azimuth, with a circular standard deviation of 54.21°, and a 95% confidence interval of 90.78° and 50.53° (Fig. 3). The relatively low circular variance (0.36, where 0 is unimodal and 1 evenly distributed around a circle) supports the predominant unidirectional deposition of the bones (Morris et al., 1996). The distal portions of some bones are eroded or broken (e.g. the distal portion of the femur MCD-4698, Fig. 7), while other elements preserve delicate structures (e.g. the obturator process of the ischium MCD-6689, Fig. 6B). The different preservation state of the bones suggests that the depositional event was driven by a quick unidirectional flow (Morris et al., 1996).

3. Material and methods

3.1. Material

169 The hadrosaurid remains collected from Els Nerets consists of a partial dentary tooth
170 (MCD-5214), six partial dorsal vertebrae (MCD-8632, MCD-8633, MCD-8634, MCD-8635,
171 MCD-8636, MCD-8637), a sacral centrum (MCD-64), two fused sacral centra (MCD-7027),
172 complete proximal caudal vertebra (MCD-8638), complete caudal vertebrae (MCD-6690,
173 IPS-NE-13), seven partial caudal vertebrae (MCD-61, MCD-62, MCD-63, MCD-65, MCD-
174 66, MCD-5209, MCD-7095), complete left humerus (MCD-6691), right ulna (MCD-8640),
175 fragment of left radius (MCD-5208), fragment of left ilium (MCD-8639), nearly complete
176 right ischium (MCD-6689), partial left ischium (MCD-7032), two complete right femora
177 (MCD-4698, 7033), partial distal half of right femur (IPS-896), distal epiphysis of left femur
178 (MCD-6743b), partial right fibula (MCD-6688), and fragmentary right metatarsal IV (MCD-
179 5203). The material belongs to at least three individuals, based on the recovery of a maximum
180 of three right femora.
181
182 *3.2. Phylogenetic analysis*
183 The phylogenetic position of the Els Nerets lambeosaurine was inferred using
184 Maximum Parsimony analysis. The taxonomic sample included 16 non hadrosaurid-
185 hadrosauroids, 23 Saurolphinae and 24 Lambeosaurinae. We used the character-taxon matrix
186 of Prieto-Márquez et al. (2019), to which we added five new characters (Appendix), totalling
187 285 morphological characters (195 cranial and 90 postcranial; see supplementary data 1 and
188 2). The tree search was conducted in TNT version 1.5 (Goloboff and Catalano, 2016). A
189 heuristic search of 10,000 replicates using random addition sequences was performed,
190 followed by branch swapping by tree bisection reconnection holding ten trees per replicate.
191 Multistate characters containing states that are not mutually exclusive, following a natural
192 morphocline, were ordered. Bootstrap proportions (Felsenstein, 1985) were calculated using
193 TNT, setting the analysis for 5,000 replicates using heuristic searches, in which each search

was conducted using random additional sequences with branch-swapping by subtree pruning and regrafting and 25 replicates.

4. Results

4.1. Cranial elements

The only cranial element recovered at Els Nerets, MCD-5214, is a dentary tooth crown missing the apical region (Fig. 4). The tooth crown is diamond-shaped, as is typical of hadrosaurids (Prieto-Márquez, 2010), slightly asymmetrical and gently curved caudally. Assuming that the dorsal half of the crown was as tall as the preserved ventral half, the element was about three times taller than wide at mid-height. The enamelled surface bears a single median ridge the lingual margin of which is eroded away along its dorsal extent. Two or three short fainter accessory ridges are present on each side of the much larger and robust median ridge (Fig. 4B). These fainter ridges are obliquely oriented relative to the median ridge and disappear before mid-height of the tooth crown. Marginal papillae are relatively small and subrectangular (Fig. 4A).

4.2. Axial elements

4.2.1. Dorsal Vertebrae

Dorsal centra (MCD-8632–MCD-8637; Table 1) are slightly opisthocoelous, gently compressed craniocaudally and mediolaterally, and with heart-shaped cranial and caudal articular surfaces (Fig. 5A and B). The description is based on the vertebra MCD-8633. The neural arch is fused to the centra. The neural canals are elliptical, more expanded dorsoventrally than mediolaterally. The prezygapophyses are elliptical facets oriented

craniodorsally laying near the craniodorsal margin of the neural arch. The transverse processes are elliptical in cross section and show a well developed ventral ridge. The ridge is attached medially to the transverse process and expands caudoventrally, articulating with the caudal margin of the neural arch. Most postzygapophyses are incompletely preserved and are oriented caudoventrally. Between the postzygapophyses there is a sulcus on the caudal margin of the neural spine. The neural spine lacks the distal portion and it has a slight cranial offset. It has an elliptical section, with a height at least twice that of the centrum.

4.2.2. Sacrum

The sacrum is incompletely known from a few fragmentary centra. MCD-7027 consists of two fused sacral centra (Fig. 5C–E). The dorsal surface preserves the peduncles of the neural arches. MCD-64 consists of a sacral centrum preserving portions of the neural arches and the attachment sites for the transverse processes (Fig. 5F–H). All these sacral centra are slightly wider than tall. They are slightly hourglass-shaped in ventral view, given that they are mediolaterally constricted at mid-length. The ventral surfaces of these centra are smooth and show no sulci.

4.2.3. Caudal Vertebrae

MCD-8638 (Fig. 5I and J) is a proximal caudal vertebra exhibiting craniocaudally compressed and opisthocoelous centra, with concave lateral surfaces. The neural arch encloses an oval neural canal. Above and between both prezygapophyses, on the cranial surface of the base of the neural spine, there is a wide sulcus that narrows dorsally. The transverse processes are dorsoventrally expanded, craniocaudally compressed and slightly offset cranially. Dorsal to the neural canal, the postzygapophyses are elliptical facets and oriented ventrally. The neural spine is twice as tall as the centrum and it is caudally inclined along its proximal

segment 25° relative to the dorsoventral axis of the centrum. The neural spine is elliptical in cross section, thicker proximally than distally. On the cranial surface of the neural spine there is a sulcus above the prezygapophyses that extends to mid-height of the neural spine.

IPS-NE-13 (Fig. 5K and L) preserves the amphicoelous centrum of a mid-caudal vertebra. This centrum displays hexagonal cranial and caudal facets, and concave lateral and ventral surfaces. The ventral surface preserves the articular facets for the haemal arches. The lateral surfaces bear approximately square facets for attachment of the transverse processes. These facets are more expanded craniocaudally than dorsoventrally. The proximal segment of the neural arch is caudally inclined and encloses a rounded neural canal. The prezygapophyses are cranially projected with craniomedially oriented articular facets. Dorsomedial to the prezygapophyses, on the cranial surface of the neural spine, there is a sulcus that extends to mid-height of the neural spine. The postzygapophyses are relatively small, located on the neural spine, dorsal to the neural canal and facing lateroventrally. The neural spine is slightly inclined caudally, missing its distal end and is less than twice the height of the centrum.

MCD-6690 is a highly distorted mid-caudal vertebra (Fig. 5M–P), diagenetically compressed mediolaterally. The centrum is amphicoelous and the proportions and dimensions of the articular facets have not been distorted. The lateral surfaces are concave. The right surface shows the articular facet for the transverse process. The ventral surface of the centrum is concave, with a smooth median sulcus. The neural arch is poorly preserved and encloses a rounded neural canal. Dorsal to the neural canal, the prezygapophyses show an oval shape and face craniodorsally. The neural spine is more than three times taller than the centrum and it expands and thickens distally. Dorsal to the prezygapophyses, on the cranial surface of the neural spine, there is a small sulcus (Fig. 5N). On the cranial surface of the neural spine, 5 cm above the attachment of the neural arch, there is a rounded and short protuberance that extends cranially (Fig. 5O and P). This feature is anomalous in that it is not present in any of

the other available vertebrae for which the neural spine is preserved, nor is it known in any other ornithopod for that matter. Given its anomalous shape and location, we suggest that it may be pathological. However, because the bone surface of this feature is smooth, as that of the lateral surface of the neural spine, it is likely not the result of bone fracture and remodelling, but rather perhaps an abnormality that might have been present from birth.

4.3. Appendicular elements

4.3.1. Humerus

MCD-6691 is a well preserved left humerus (Fig. 6A–C) missing only small portions of the cranial margin of the deltopectoral crest. This is a particularly slender element, more than five times longer than wide (the width here being measured along the proximal margin of the lateral surface). This ratio makes MCD-6691 one of the more gracile humeri of a lambeosaurine. The lateral surface of the expanded proximal end describes a slightly concave outline in proximal view, with the proximal extent of the deltopectoral crest oriented craniolaterally. The deltopectoral crest accounts for 57% of the length of the humerus. The lateroventral expansion of the crest is 1.7 times the minimum diameter of the shaft. The shaft of the humerus exhibits a slightly sigmoidal profile in mediolateral view. Distally, the shaft expands both craniomedially and caudolaterally to form the distal condyles. The two condyles are oval in cross section, the radial condyle being slightly more robust than the ulnar condyle. The condyles are separated by a deep sulcus that is further developed caudally.

4.3.2. Ulna

MCD-8640 is an almost complete right ulna (Fig. 6D and E). It has a slender diaphysis, being more than 14 times longer than it is dorsoventrally thick. At the proximal end, the lateral and medial flanges are heavily eroded. The olecranon process is relatively thick mediolaterally and its proximal surface is abraded. The dorsal surface of the proximal segment of the ulna displays a shallow depression that occupies half the length of the bone. The diaphysis exhibits longitudinal shallow striated ligament scars. The distal end is eroded and shows an oval section.

4.3.3. Radius

This element is solely represented by an eroded fragment of a left distal end (MCD-5208; Fig. 6F and G). The distal surface is subcircular. The distal-most region of the diaphysis is suboval in cross section and shows longitudinal striated ligament scars.

4.3.4. Ilium

MCD-8639 is a proximal segment of the preacetabular process of a left ilium (Fig. 7A). The process is an elongate lamina that gradually becomes slightly shallower distally. The proximal extent of the preserved segment curves ventrally and is broken before reaching the craniodorsal margin of the pubic process of the ilium. On the medial surface there is a longitudinal ridge, a condition shared among all hadrosaurids (Prieto-Márquez 2010).

4.3.5. Ischium

The right ischium MCD-6689 (Fig. 7B–E) is nearly complete, missing only the distal end. The element exhibits a 'thumb-like' iliac processes. The dorsal and ventral margins of the iliac process are convergent. The pubic process of MCD-6689 is relatively elongated, being as long as it is wide along its articular face. The obturator process appears relatively

318 long and thin due to erosion and breakage. The shaft of the ischium is relatively slender: its
319 dorsoventral thickness at mid-length is 5.4% of its total length. A depression is present on the
320 lateral surface of the proximal extent of the shaft. Ventrally, this depression is bounded by a
321 sharp ridge. On the medial surface, there are several longitudinal ridges for the articulation
322 with its counterpart.

323 The left ischium MCD-7032 is slightly distorted post-depositionally and lacks portions
324 of the pubic and iliac processes, the obturator process and the distal end. The iliac process is
325 'thumb-shaped' in lateral profile and displays the same proportions as MCD-6689. On the
326 lateral surface of the ischium, also as in MCD-6689, there is a depression. This depression is
327 located caudal and ventral to the iliac process, delimited by a ridge at the level of the obturator
328 process. The ischiatic shaft is slightly deformed, and on the medial surface there are ridges
329 indicating articulation with its counterpart.

330

331 *4.3.6. Femur*

332 The femur is the best represented appendicular element of the lambeosaurine from Els
333 Nerets. The following description is mostly based on the two complete femora, MCD-7033
334 (Fig. 8A–B) and MCD-4698 (Fig. 8C–D). MCD-7033, previously referred to the nomen
335 dubium *Orthomerus* (Casanovas et al., 1985), is a complete right femur, albeit diagenetically
336 compressed mediolaterally. The articular head is compressed craniocaudally but preserves the
337 dimension proximodistally. The forth trochanter displays a symmetrical profile in lateral view
338 and is continuous with the lateral margin of the shaft. The distal condyles, the more robust of
339 which is the medial one, form an 'H' shape in distal view. The lateral condyle presents a
340 concave lateral surface. The gentle curvature of the shaft and the symmetrical profile of the
341 fourth trochanter demonstrate that referring this femur to the genus *Orthomerus* is erroneous,

since the femora of *Orthomerus dolloi* Selley, 1883, the only recognized species of the genus, show different features.

MCD-4698 is the best preserved femur from Els Nerets. It is comparable in size (length: 63 cm) with the medium sized femora from the Basturs Poble site (Dalla Vecchia et al., 2014; Fondevilla et al., 2018). The greater trochanter is craniocaudally expanded, with a concave lateral surface. The shaft has a gentle curvature and a squared cross section. The fourth trochanter is well preserved, with a symmetrical profile, and its length corresponds to 30% of the total length of the femur.

4.3.7. Fibula

MCD-6688 is a rod-like right fibula (Fig. 8E–F), with a smooth curvature along the distal half of the bone. The proximal half of the shaft is slightly expanded, maintaining a triangular section that becomes circular distally.

4.3.8. Metatarsal IV

MCD-5203 is a proximal fragment of a right metatarsal IV (Fig. 8G–H). Except for its dorsolateral surface, all other sides are eroded to the point of exposing the inner osseous texture. The partially preserved medial surface appears to have been gently depressed, for articulation with the metatarsal III. The incomplete distal portion displays a D-shaped section.

4.4. Phylogenetic relationships of the Els Nerets lambeosaurine

The Maximum Parsimony analysis resulted in 12 most parsimonious trees hitting a best score of 1071 steps for 1909 times out of 10000 replicates; with Consistency Index of 0.45 and Retention Index of 0.77. The consensus tree placed the Els Nerets lambeosaurine within Lambeosaurinae, forming a polytomic relationship with the basal lambeosaurine

367 species *Aralosaurus tubiferus*, *Canardia garonnensis*, *Jaxartosaurus aralensis*, *Tsintaosaurus*
368 *spinorhinus*, *Pararhabdodon isonensis* and *Adynomosaurus arcanus* (Fig. 9).
369 Lambeosaurine synapomorphies present in the Els Nerets specimens consist of a long
370 deltopectoral crest that is over 55% of the length of the humerus, and a recurved 'thumb-like'
371 iliac process. The Els Nerets lambeosaurine shares with Tsintaosaurini a pubic process as long
372 as its articular surface is wide, and an ischium with mid-shaft depth being less than 7.5% of
373 the length of the shaft.
374
375 **5. Discussion**
376
377 *5.1. Comparison with other lambeosaurines*
378 The dorsal vertebrae of the Els Nerets lambeosaurine show a sulcus between the
379 postzygapophyses on the caudal margin of the neural spine of the dorsal vertebrae, which is
380 present in all members of the clade except *Amurosaurus riabini* Bolotsky & Kurzanov, 1991
381 (Godefroit et al., 2004). The height of the neural spine relative to the centrum of dorsal
382 vertebrae is similar to those of most Lambeosaurinae, except *Magnapaulia laticaudus*, Prieto-
383 Márquez et al., 2012 (e.g. LACM 17715), *Hypacrosaurus* spp. (e.g. MOR 549, CMN 8501)
384 and *Arenysaurus ardevoli* Pereda-Suberbiola et al., 2009 (MPZ2008/268, Cruzado-Caballero
385 et al., 2013), which display taller neural spines. The absence of a ridge on the cranial surface
386 of the neural spine is shared with other lambeosaurines, such as *Tsintaosaurus spinorhinus*
387 Young, 1958 (e.g. IVPP V725), *Parasaurolophus walkeri* Parks, 1922 (e.g. ROM 768),
388 *Lambeosaurus lambei* Parks, 1923 (e.g. ROM 758) and *Hypacrosaurus* spp. (e.g. MOR 549,
389 CMN 8501). Caudal vertebrae show relative proportions of the centrum and the neural spine
390 that are similar to those described in other Lambeosaurinae, such as tsintaosaurins
391 *Tsintaosaurus spinorhinus* (e.g. IVPP V725) and *Pararhabdodon isonensis* (IPS SRA 24,

392 Prieto-Márquez et al., 2006), and lambeosaurins *Corythosaurus* spp. (e.g. LACM 126137),
393 *Lambeosaurus lambei* (e.g. ROM 758) and *Parasaurolophus* spp. (e.g. ROM 768, FNMH
394 P27393). On the cranial surface of the neural spine, a sulcus above the prezygapophyses that
395 extends to mid-height of the neural spine is shared with all other lambeosaurines, except
396 *Olorotitan ararhensis* Godefroit et al., 2003 (e.g. AEMH 2/845, Godefroit et al., 2012).
397 In the humerus, a deltopectoral crest accounting for over 55% of its length is also
398 present in most lambeosaurines (Prieto-Márquez 2010), with the exception of *Canardia*
399 *garonnensis* (MDE-Ma3-20, Prieto-Márquez et al., 2013) and *Charonosaurus jiayinensis*
400 (Godefroit et al., 2000). Similar proportions of the lateroventral expansion of the deltopectoral
401 crest relative to the shaft diameter have been reported only in *Magnapaulia laticaudus* (e.g.
402 LACM 17715, Prieto-Márquez et al., 2012) among lambeosaurines.
403 The ischia recovered from Els Nerets show a 'thumb-like' iliac process, a common
404 character among Lambeosaurinae (Brett-Surman and Wagner, 2007). The length/width ratio is
405 similar to that of all other lambeosaurines, with values between 1.5 and 2, except in
406 *Parasaurolophus cyrtocristatus* Ostrom, 1961 (e.g. FMNH P27393) which is less than 1.5,
407 and *Amurosaurus riabinini* (Godefroit et al., 2004) which is greater than 2. The dorsal and
408 ventral margins of the iliac process are convergent, and the articular facet has a length/width
409 ratio less than 0.7; these characters are different from *Adynomosaurus arcanus* (e.g. MCD-
410 7139). The elongated pubic process is a condition only shared with *Tsintaosaurus spinorhinus*
411 (e.g. IVPP V725) and *Parasaurolophus cyrtocristatus* (e.g. FMNH P27393). The proportions
412 of shaft width at mid-length relative to its total length, having a ratio between 0.05 and 0.075,
413 is a condition shared with *T. spinorhinus* (e.g. IVPP V725), *Hypacrosaurus stebingeri* Horner
414 and Currie, 1994 (e.g. MOR 549), *Lambeosaurus lambei* (e.g. ROM 1218), *Olorotitan*
415 *ararhensis* (e.g. AEMH 2/845), *Parasaurolophus walkeri* Parks, 1922 (e.g. ROM 768),
416 *Sahalyania elunchunorum* Godefroit et al., 2008 (e.g. GMH W400-2) and *Velafrons*

417 *coahuilensis* Gates et al., 2007 (e.g. CPC-59). The depression on the lateral surface of the
418 ischium is present in all lambeosaurines except *Magnapaulia laticaudus* (e.g. LACM 17715),
419 *Velafrons coahuilensis* (uncatalogued ischium from Cerro del Pueblo Formation examined at
420 the Museo del Desierto, Saltillo) and *Sahaliyania elunchunorum* (e.g. GMH W400-2).
421
422 *5.2. Comparison with lambeosaurines from Europe*
423 Unlike other European lambeosaurine species (e.g. Casanovas-Cladellas et al., 1993),
424 the Els Nerets form is characterized by lacking a cranial ridge on the neural spine of dorsal
425 vertebrae. Likewise, the overall length/width proportions of the humerus are different: a ratio
426 greater than 5 is recovered in the Els Nerets lambeosaurine while it is smaller than 4.9 in *P.*
427 *isonensis*. The Els Nerets lambeosaurine is characterized by having a length/width ratio of the
428 articular facet of the ischiadic iliac process smaller than 0.7 and convergent margins of the
429 iliac process, while *Adynomosaurus arcanus* is characterized by having a wider articular facet
430 and divergent margins. The Els Nerets specimen shares three characters with the
431 lambeosaurine from the nearby Moror locality (Brinkmann, 1984) and *Tsintaosaurus*
432 *spinorhinus*, namely a length/width ratio of the iliac process between 1.5 and 2, convergent
433 caudodorsal and acetabular margins of the iliac process, and a depression of the lateral surface
434 of the proximal ischiadic shaft.
435 Dorsal and sacral vertebrae (for which the neural spine is preserved) from Els Nerets
436 differ from those of *Arenysaurus ardevoli* in having neural spines that are 3.25 times taller
437 than their centra, the absence of a ridge on the cranial surface of the neural spine of dorsal
438 vertebrae, and a sulcus on the cranial surface of the neural spine of caudal vertebrae.
439 Prieto-Márquez and Wagner (2009) and Prieto-Márquez et al. (2013) diagnosed the
440 tribe Tsintaosaurini based on maxillary characters, none of which are preserved in Els Nerets.
441 However, the aforementioned ischiadic characters shared between Els Nerets and

442 *Tsintaosaurus* hint at a possible relationship between those two forms, although this is not
443 unambiguously supported by phylogenetic analysis.
444
445 *5.3 The arrival of lambeosaurines in Europe*
446 The only European region where lambeosaurine dinosaurs have been reported is the
447 Ibero-Armorican island (Pereda-Suberbiola et al., 2009; Cruzado-Caballero et al., 2010;
448 Prieto-Márquez et al., 2013; Csiki et al., 2015; Fondevilla et al., 2019). Prieto-Márquez and
449 Wagner (2009) and Prieto-Márquez et al. (2013) reported the presence in the late
450 Maastrichtian of members of tsintaosaurin (*Pararhabdodon isonensis*) and aralosaurin
451 (*Canardia garonnensis*) tribes, respectively. The authors inferred that they were Asian
452 immigrants which apparently would have reached the Ibero-Armorican island via dispersal
453 events at the end of the early Maastrichtian or during the late Maastrichtian (Prieto-Márquez
454 et al., 2013). The occurrence of other lambeosaurines with their closest relatives in North
455 America (Csiki et al., 2015) led some authors to speculate that several migratory events
456 occurred in the late Maastrichtian: two bringing tsintaosaurins and aralosaurins from Asia
457 (Prieto-Márquez et al. 2013) and two other events bringing parasaurolophins from Asia into
458 Europe and North America (Cruzado-Caballero et al., 2013). Although tentative, the apparent
459 affinity of the Els Nerets lambeosaurine with *Tsintaosaurus spinorhinus* may provide support
460 for an early Maastrichtian arrival of tsintaosaurins in the region (about 4 My before the
461 occurrence of the tsintaosaurine *Pararhabdodon* in the latest Maastrichtian) and therefore, the
462 timing and palaeogeographic origin of the early migratory event.
463 Furthermore, the Els Nerets lambeosaurine represents the first occurrence of
464 Lambeosaurinae in Europe, and in particular those with Asian affinities. The early
465 Maastrichtian arrival of lambeosaurines in western Europe sets the timing of the ecological
466 change and community reorganization occurring during the so-called “Maastrichtian dinosaur

turnover" (Vila et al. 2016). Subsequently, lambeosaurine hadrosaurids rapidly became the most abundant herbivorous group in the late early Maastrichtian (Vila et al., 2016). Interestingly, the appearance of lambeosaurine hadrosaurids in the late early Maastrichtian (around 70 Ma) coincides with marine isotopic events 4 and 5 of the Campanian-Maastrichtian Boundary Events (CMBE) that could have brought about an important sea level drop (up to 25 m) which in turn would have favoured the opening of passages between landmasses (Fondevilla et al., 2019).

6. Conclusions

We document and re-evaluate the affinities of the hadrosaurid material from the classic European locality of Els Nerets, in the Tremp Basin (Catalonia). This lambeosaurine represents the oldest record of this clade in Europe. Several pelvic characters indicate a possible relationship with the Asian *Tsintaosaurus*. This, combined with the updated chronostratigraphic position of the site (c. 70 Ma), provides support for the hypothesis that tsintaosaurins arrived in Europe no later than early Maastrichtian. Future studies should test the tsintaosaurin affinities of Els Nerets and other south Pyrenean hadrosaurids, and a long history of this lineage in western Europe.

Acknowledgements

We thank Rodrigo Gaete, Fabio Marco Dalla Vecchia, Victor Fondevilla and Cristiano Dal Sasso for providing additional data on specimens collected from various localities at the eastern Tremp syncline and elsewhere in Europe. We are also grateful to the numerous volunteers who took part in the fieldwork at Els Nerets. Thanks also to two anonymous

reviewers whose comments improved the quality of the manuscript. This work was supported by the Ministry of Economy, Industry and Competitivity of the Government of Spain, via the Ramón y Cajal Program [RyC-2015-17388] presented to A. P.-M. and a grant [CGL2016-73230-P] presented to A. G. Additional support was also provided by the CERCA Program of the Generalitat de Catalunya, and the University of Bristol through the Bob Savage Memorial Fund.

Supplementary data

Supplementary data 1. Taxon-character state matrix used in the phylogenetic analysis.

References

Benton, M.J., Csiki, Z., Grigorescu, D., Redelstorff, R., Sander, P.M., Stein, K., Weishampel, D.B., 2010. Dinosaurs and the island rule: the dwarfed dinosaurs from Haţeg Island. Palaeogeography, Palaeoclimatology, Palaeoecology 293, 438–454. doi: 10.1016/j.palaeo.2010.01.026

Blanco, A., Szabó, M., Blaco-Lapaz, À., Marmi, J., 2017. Late Cretaceous (Maastrichtian Chondrichtyes and Osteichtyes from northeastern Iberia. Palaeogeography, Palaeoclimatology, Palaeoecology 465, 278–294. doi: 10.1016/j.palaeo.2016.10.039

Bolotsky, Y., Kurzanov, S.M., 1991. Gadrosavry Priamuriy. Geology of the Pacific Ocean Border, 94–103.

Brett–Surman, M.K., Wagner, J.R., 2007. Discussion of character analysis of the appendicular anatomy in Campanian and Maastrichtian North American hadrosaurids – variation and

516 ontogeny. In: Carpenter, K. (Ed.), Horns and Beaks: Ceratopsian and Ornithopod
517 Dinosaurs. Indiana University Press, Bloomington and Indianapolis, 135–169.
518 Brinkmann, W., 1984. Erster Nachweis eines Hadrosauriers (Ornithischia) aus dem unterem
519 Garumnium (Maastrichtium) des Beckens von Tremp (Provinz Lérida, Spanien).
520 Paläontologische Zeitschrift 58, 295–305.
521 Brinkmann, W., 1988. Zur Fundgeschichte und Systematik der Ornithopoden (Ornithischia,
522 Reptilia) aus der ober-Kreide von Europe. Documenta Naturae 45, 1–157.
523 Buffetaut, E., 2009. An additional hadrosaurid specimen (Dinosauria: Ornithischia) from the
524 marine Maastrichtian deposits of the Maastricht area. Carnets de Géologie (L03), 1–4.
525 Canudo, J.I., Oms, O., Vila, B., Galobart, À., Fondevilla, V., Puértolas-Pascual, E., Sellés, A.
526 G., Cruzado–Caballero, P., Dinarès-Turell, J., Vicens, E., Castanera, D., Company, J.,
527 Burrel, L., Estrada, R., Marmi, J., and Blanco, A., 2016. The upper Maastrichtian
528 dinosaur fossil record from the southern Pyrenees and its contribution to the topic of the
529 Cretaceous-Palaeogene mass extinction event. Cretaceous Research 57, 540–551.
530 Casanovas-Cladellas, M.L., Santafé-Llopis, J.V., Sanz, J.L., Buscalioni, A., 1985.
531 *Orthomerus* (Hadrosaurinae, Ornithopoda) del Cretácico Superior del yacimiento de "Els
532 Nerets" (Tremp, España). Paleontologia i Evolució 19, 155–162.
533 Casanovas, M.L., Santafé-Llopis, J.V., Sanz, J.L., Buscalioni, A.D., 1987. Arcosaurios
534 (Crocodilia, Dinosauria) del Cretacico Superior de la Conca de Tremp (Lleida, España).
535 Estudios Geologicos, vol. extr. Galve-Tremp, 95–110.
536 Casanovas-Cladellas, M.L., Santafé-Llopis, J.V., Isidro-Llorens, A., 1993. *Pararhabdodon*
537 *isonense* n. gen. n. sp. (Dinosauria). Estudio morfológico, radiotomográfico y
538 consideraciones biomecanicas. Paleontologia i Evolució 26–27, 121–131.

539 Company, J., Cruzado-Caballero, P., Canudo, J.I., 2015. Presence of diminutive hadrosaurids
540 (Dinosauria: Ornithopoda) in the Maastrichtian of the south–central Pyrenees (Spain).
541 Journal of Iberian Geology 41, 71–81.
542 Cruzado-Caballero, P., Pereda-Superbiola, X., Ruiz-Omeñaca J.I., 2010. *Blasisaurus canudoi*
543 gen. et sp. nov., a new lambeosaurine dinosaur (Hadrosauridae) from the latest
544 Cretaceous of Arén (Huesca, Spain). Canadian Journal of Earth Sciences 47, 1507–1517.
545 Cruzado-Caballero, P., Canudo, J.I., Moreno-Azanza, M., Ruiz-Omeñaca J.I., 2013. New
546 material and phylogenetic position of *Arenysaurus ardevoli*, a lambeosaurine dinosaur
547 from the Late Maastrichtian of Arén (Northern Spain). Journal of Vertebrate
548 Paleontology 33, 1367–1384.
549 Csiki-Sava, Z., Buffetaut, E., Ősi, A., Pereda-Superbiola, X., Brusatte, S. L., 2015. Island life
550 in the Cretaceous – faunal composition, biogeography, evolution, and extinction of land-
551 living vertebrates on the Late Cretaceous European archipelago. ZooKeys, 469, 1–161.
552 doi: 10.3897/zookeys.469.8439
553 Cuevas, J.L., 1992. Estratigrafia del "Garumniense" de la Conca de Tremp. Prepirineo de
554 Lerida. Acta Geológica Hispánica 27, 95–108.
555 Dalla Vecchia, F.M., 2014. An overview of the latest Cretaceous hadrosauroid record in
556 Europe. In: Eberth, D.A., Evans, D.C. (Eds.), Hadrosaurs. Indiana University Press,
557 Indianapolis, 268–297.
558 Dalla Vecchia, F.M., Gaete, R., Riera, V., Oms, O., Prieto-Márquez, A., Vila, B., Sellés,
559 A.G., Galobart, A., 2014. The hadrosauroid record in the Maastrichtian of the eastern
560 Tremp Syncline (northern Spain). In: Eberth, D.A., Evans, D.C. (Eds.), Hadrosaurs.
561 Indiana University Press, Indianapolis, 298–314.
562 Díez-Canseco, D., Arz, J.A., Benito, M., Diaz-Molina, M., Arenillas, I., 2014. Tidal influence
563 in redbeds: a palaeoenvironmental and biochronostratigraphic reconstruction of the

564 Lower Tremp Formation (South-Central Pyrenees, Spain) around the Cretaceous/
565 Paleogene boundary. Sedimentary Geology 312, 31–49. doi:
566 10.1016/j.sedgeo.2014.06.008
567 Felsenstein, J., 1985. Confidence limits on phylogenies: an approach using the bootstrap.
568 Evolution 39, 783–791.
569 Fondevilla, V., Vincente, A., Battista, F., Sellés, A.G., Dinarès-Turell, J., Martínclosas, C.,
570 Anadón, P., Vila, B., Razzolini, N.L., Galobart, À., Oms, O., 2017. Geology and
571 taphonomy of the L'Espinau dinosaur bonebed, a singular lagoonal site from the
572 Maastrichtian of the South–Central Pyrenees. Sedimentary Geology 355, 75–92.
573 Fondevilla, V., Dalla Vecchia, F.M., Gaete, R., Galobart, À., Moncunill–Solé, B., Köhler, M.,
574 2018. Ontogeny and taxonomy of the hadrosaur (Dinosauria, Ornithopoda) remains from
575 Basturs Poble bonebed (late early Maastrichtian, Tremp syncline, Spain). PLoS ONE
576 13(10): e0206287. doi: 10.1371/journal.pone.0206287
577 Fondevilla, V., Riera, V., Vila, B., Sellés, A.G., Dinarès-Turell, J., Vicens, E., Gaete, R.,
578 Oms, O., Galobart, À., 2019. Chronostratigraphic synthesis of the latest Cretaceous
579 dinosaur turnover in south–western Europe. Earth-Science Reviews 191, 168–189. doi:
580 10.1016/j.earscirev.2019.01.007
581 Gates, T.A., Sampson, S.D., Delgado de Jesus, C.R., Zanno, L.E., Eberth, D., Hernandez-
582 Rivera, R., Aguillon-Martinez, M.C., 2007. *Velafrons coahuiulensis*, a new
583 lambeosaurine hadrosaurid (Dinosauria: Ornithopoda) from the Late Campanian Cerro
584 del Pueblo Formation, Coahuila, Mexico. Journal of Vertebrate Paleontology 27, 917–
585 930.
586 Godefroit, P., Zan, S., Jin, L., 2000. *Charonosaurus jiayinensis* n. g., n. sp., a lambeosaurine
587 dinosaur from the Late Maastrichtian of northeastern China. Comptes Rendus de
588 l'Academie des Sciences, Paris, Sciences de la Terre et des Planètes 330, 875–882.

589 Godefroit, P., Bolotsky, Y., Alifanov, V., 2003. A remarkable hollow-crested hadrosaur from
590 Russia: an Asian origin for lambeosaurines. Comptes Rendus Palevol 2, 143–151.
591 Godefroit, P., Bolotsky, Y.L., van Itterbeek, J., 2004. The lambeosaurine dinosaur
592 *Amurosaurus riabini*, from the Maastrichtian of Far Eastern Russia, Acta Palaeontologica
593 Polonica 49, 585–618.
594 Godefroit, P., Sjulin, H., Tingxiang, Y., Lauters, P., 2008. New hadrosaurid dinosaurs from
595 the uppermost Cretaceous of northeastern China. Acta Palaeontologica Polonica 53, 47–
596 74.
597 Godefroit, P., Bolotsky, Y.L., Bolotsky, I.Y., 2012. Osteology and relationships of *Olorotitan*
598 *arharensis*, a hollow–crested hadrosaurid dinosaur from the latest Cretaceous of Far
599 Eastern Russia. Acta Palaeontologica Polonica 57, 527–560.
600 Goloboff, P.A., Farris, J.S., Nixon, K.C., 2008. TNT, a free program for phylogenetic
601 analysis. Cladistics 24, 774–786.
602 Horner, J.R., Currie, P.J., 1994. Embryonic and neonatal morphology and ontogeny of a new
603 species of *Hypacrosaurus* (Ornithischia, Lambeosauridae) from Montana and Alberta.
604 Dinosaur Eggs and Babies, Cambridge University Press, Cambridge, 312–336.
605 Horner, J.R., Weishampel, D.B., Forster, C.A., 2004. Hadrosauridae. In: Weishampel, D.B.,
606 Dodson, P., Osmólska, H. (Eds.), The Dinosauria, Second Edition. University of
607 California, Berkeley, 438–463.
608 Kovach, W., 2018. Oriana version 4.02. Kovach Computing Services, Anglesey, Wales.
609 Mey, P.H., Nagtegaal, P.J.C., Roberti, K.J.A., Hartelvelt, J.J.A., 1968. Lithostratigraphic
610 subdivision of posthercynian deposits in the south–central Pyrenees, Spain. Leidse
611 Geologische Mededelingen 41, 221–228.

612 Morris, T.H., Richmond, D.R., Grimshaw, S.D., 1996. Orientation of dinosaur bones in
613 riverine environments: insights into sedimentary dynamics and taphonomy. In Morales,
614 M., ed., The Continental Jurassic: Museum of Northern Arizona Bulletin 60, 521–530.
615 Ostrom, J.H., 1961. A New Species of hadrosaurian dinosaur from the Cretaceous of New
616 Mexico. Journal of Vertebrate Paleontology 35, 575–577.
617 Parks, W.A., 1922. *Parasaurolophus walkeri*, a new genus and species of crested trachodont
618 dinosaur. University of Toronto Studies, Geology Series 13, 1–32.
619 Parks, W.A., 1923. *Corythosaurus intermedius*, a new species of trachodont dinosaur.
620 University of Toronto Studies, Geological Series 15, 1–57.
621 Pereda-Superbiola, X., Canudo, J.I., Cruzado-Caballero, P., Barco, J.L., López-Martínez, N.,
622 Oms, O., Ruiz-Omeñaca, J.L., 2009. The last hadrosaurid dinosaurs of Europe: a new
623 lambeosaurine from the uppermost Cretaceous of Aren (Huesca, Spain). Comptes Rendus
624 Palevol 8, 559–572.
625 Prieto-Márquez, A., 2010. Global phylogeny of Hadrosauridae (Dinosauria: Ornithischia)
626 using parsimony and Bayesian methods. Zoological Journal of the Linnean Society 15,
627 435–502.
628 Prieto-Márquez, A., Gaete, R., Rivas, G., Galobart, À., Boada, M., 2006. Hadrosaurid
629 dinosaurs from the Late Cretaceous of Spain: *Pararhabdodon isonensis* revisited and
630 *Koutalisaurus kohlerorum*, gen. et sp. nov. Journal of Vertebrate Paleontology 26, 929–
631 943.
632 Prieto-Márquez, A., Chiappe, L.M., Joshi, S.H., 2012. The lambeosaurine dinosaur
633 *Magnapaulia laticaudus* from the Late Cretaceous of Baja California, Northwestern
634 Mexico. PLoS ONE 7(6): e38207. doi: 10.1371/journal.pone.0038207
635 Prieto-Márquez, A., Dalla Vecchia, F.M., Gaete, R., Galobart, A., 2013. Diversity,
636 relationships, and biogeography of the lambeosaurine dinosaurs from the European

637 Archipelago, with description of the new aralosaurin *Canardia garonnensis*. PLoS ONE,
638 8(7), e69835. doi: 10.1371/journal.pone.0069835.
639 Prieto-Márquez, A., Fondevilla, V., Sellés, A.G., Wagner, J.R., Galobart, À., 2019.
640 *Adynomorsaurus arcanus*, a new lambeosaurine dinosaur from the Late Cretaceous Ibero-
641 Armorican Island of the European Archipelago, Cretaceous Research 95, 19–37.
642 Puértolas-Pascual, E., Arenillas, I., Arz, J.A., Calvin, P., Esquerro, L., García-Vicente, C.,
643 Pérez-Pueyo, M., Sánchez-Moreno, E.M., Villalaín, J.J., and Canudo, J.I., 2018.
644 Chronostratigraphy and new vertebrate sites from the upper Maastrichtian of Huesca
645 (Spain), and their relation with the K/Pg boundary. Cretaceous Research 89, 36–59.
646 Riera, V., Oms, O., Gaete, R., Galobart, À., 2009. The end-Cretaceous dinosaur succession in
647 Europe: the Tremp Basin record (Spain). Palaeogeography, Palaeoclimatology,
648 Palaeoecology 283, 160–171. doi: 10.1016/j.palaeo.2009.09.018
649 Rosell, J., Linares, R., Llompart, C., 2001. El "Garumniense" prepirenaico. Revista de la
650 Sociedad Geológica de España 14, 47–56.
651 Torices, A., Barroso-Barcenilla, F., Cambra-Moo, O., Pérez-García, A., Segura, M., 2012.
652 Palaeontological and palaeobiogeographical implications of the new Cenomanian site
653 "Algora". Cretaceous Research 37, 231–239. doi: 10.1016/j.cretres.2012.04.004
654 Vila, B., Sellés, A.G., Brusatte, S.L., 2016. Diversity and faunal changes in the latest
655 Cretaceous dinosaur communities of southwestern Europe. Cretaceous Research 57, 552–
656 564. doi: 10.1016/j.cretres.2015.07.003
657 Villalba-Breva, S., Martín-Closas, C., 2013. Upper Cretaceous paleogeography of the Central
658 Southern Pyrenean Basins (Catalonia, Spain) from microfacies analysis and charophyte
659 biostratigraphy. Facies 59, 319–345.
660 Young, C.C., 1958. The dinosaurian remains of Laiyang, Shantung. Palaeontologia Sinica,
661 New Series C 42, 1–138.

Appendix

New characters added to the character-taxon matrix of Prieto-Márquez et al. (2019) used in the phylogenetic analysis.

281. Presence or absence of ridge on the cranial surface of the neural spine of the caudal half of the dorsal vertebrae: absent (0); present (1).

282. Presence or absence of sulcus on the caudal surface of the neural spine of the caudal half of the dorsal vertebrae: absent (0); present (1).

283. Presence of absence of sulcus on the cranial surface on the neural spine of the cranial half of the caudal vertebrae: absent (0); present (1).

284. Presence or absence of depression on the lateral surface of the proximal region of the ischium. Lateral depression of the ischium: absent (0); present on the lateral surface of the ischiadic shaft (1); depression expanded in the proximal region of the ischium (2).

285. Offset of the lateral malleolus of the tibia, measured as the angle between the distal surface of the tibia and the long axis of the bone: angle greater than 12° (0); angle smaller than 12° (1).

682 **Figure captions**

683

684 **Fig. 1.** Geographical and geological location of Els Nerets site. A, geographic location of the
685 Tremp Basin (indicated by the shaded rectangle) in the Pyrenees. B, location of the main
686 hadrosaurid-bearing sites in the Eastern Tremp Basin.

687

688 Intended for a 2-column fitting image.

689

690 **Fig. 2.** Simplified stratigraphic section of the Tremp area showing the position of Els Nerets
691 site and other localities yielding lambeosaurine fossils.

692

693 Intended for a 2-column fitting image.

694

695 **Fig. 3.** Quarry map of Els Nerets site showing the spatial distribution of the recovered
696 lambeosaurine skeletal remains. The insert diagram shows the statistical distribution of the
697 angles of orientation of the fossil bones was analysed using the Orana 4.02 software (Kovach,
698 2018), with a mean orientation of 70.65° to the azimuth and the 95% confidence interval.

699

700 Intended for a 2-column fitting image.

701

702 **Fig. 4**. The only cranial element recovered from of Els Nerets lambeosaurine. A and B,
703 dentary tooth (MCD-5214) in side and lingual views, respectively.

704

705 **Fig. 5**. Axial elements of the lambeosaurine from Els Nerets. A and B, dorsal vertebra (MCD-
706 8633) in cranial and caudal views, respectively. C–E, pair of fused sacral centra (MCD-7027)

in dorsal, right lateral and ventral views, respectively. F–H, sacral centrum (MCD-64) in caudal, left lateral and ventral views, respectively. I and J, proximal caudal vertebra (MCD-8638) in cranial and left lateral views, respectively. K and L, mid-caudal vertebra (IPS-NE-13) in cranial and right lateral views, respectively. M, mid-caudal vertebra (MCD-6690) in left lateral view. N, dorsocraniolateral view of the prezygapophyseal region of MCD-6690, showing the sulcus on the cranial surface at the base of the neural spine, between the prezygapophyses. O and P, detail of the abnormal, possibly pathological growth of MCD-6690 in craniodorsal and left lateral views, respectively.

Intended for a 2-column fitting image.

Fig. 6. Forelimb elements of Els Nerets lambeosaurine. A–C, left humerus (MCD-6691) in medial, cranial, and caudolateral views, respectively. D and E, right ulna (MCD-8640) in lateral and dorsal views, respectively. F and G, distal fragment of left radius (MCD-5208) in dorsal and distal views, respectively.

Intended for a 2-column fitting image.

Fig. 7. Pelvic elements of Els Nerets lambeosaurine. A, preacetabular process of a left ilium (MCD-8639) in lateral view. B, right ischium (MCD-6689) in lateral view. C, line drawing of B. D, detail of MCD-6689 in caudoventrolateral view showing the lateral depression. E, line drawing of D.

Intended for a 2-column fitting image.

732 **Fig. 8.** Hindlimb elements of Els Nerets lambeosaurine. A and B, right femur (MCD-7033) in
733 caudolateral and cranial views, respectively. C and D, right femur (MCD-4698) in caudal and
734 craniomedial views, respectively. E and F, right fibula (MCD-6688) in caudal and cranial
735 views, respectively. G and H, proximal fragment of right metatarsal IV (MCD-5203) in
736 medial and proximal views, respectively.
737
738 Intended for a 2-column fitting image.
739
740
741 **Fig. 9.** Phylogenetic relationships of Els Nerets lambeosaurine. Shown is the strict consensus
742 tree of the 12 most parsimonious trees resulting from the parsimony analysis. Numbers below
743 branches are Bootstrap proportions.
744
745 Intended for a 2-column fitting image.
746
747
748
749

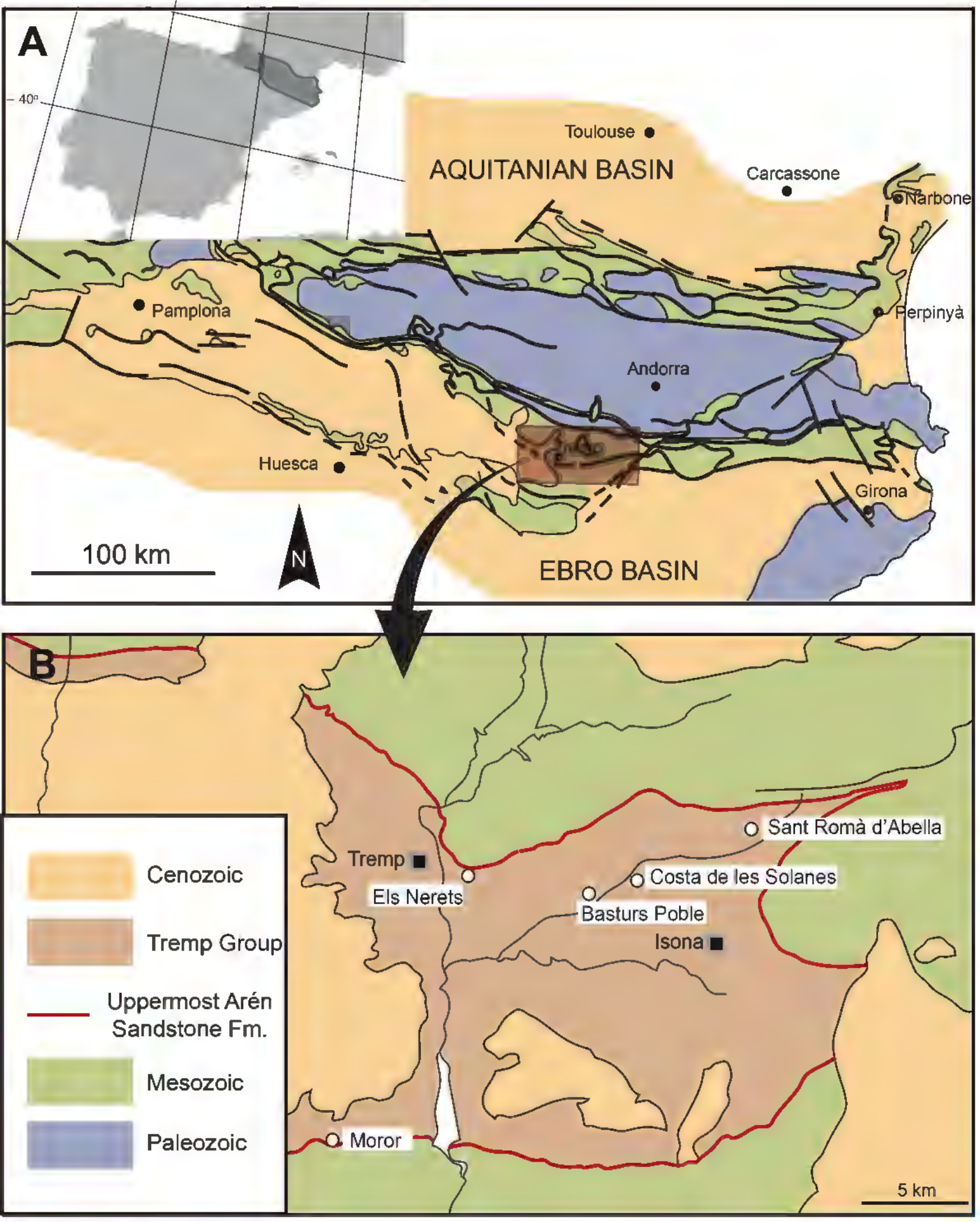
A
40°
Toulouse
AQUITANIAN BASIN
Carcassone
Narbone
Pamplona
Perpinyà
Andorra
Huesca
Girona
100 km
N
EBRO BASIN
B
Cenozoic
Tremp Group
Uppermost Arén Sandstone Fm.
Mesozoic
Paleozoic
Sant Romà d'Abella
Tremp
Costa de les Solanes
Els Nerets
Basturs Poble
Isona
Moror
5 km

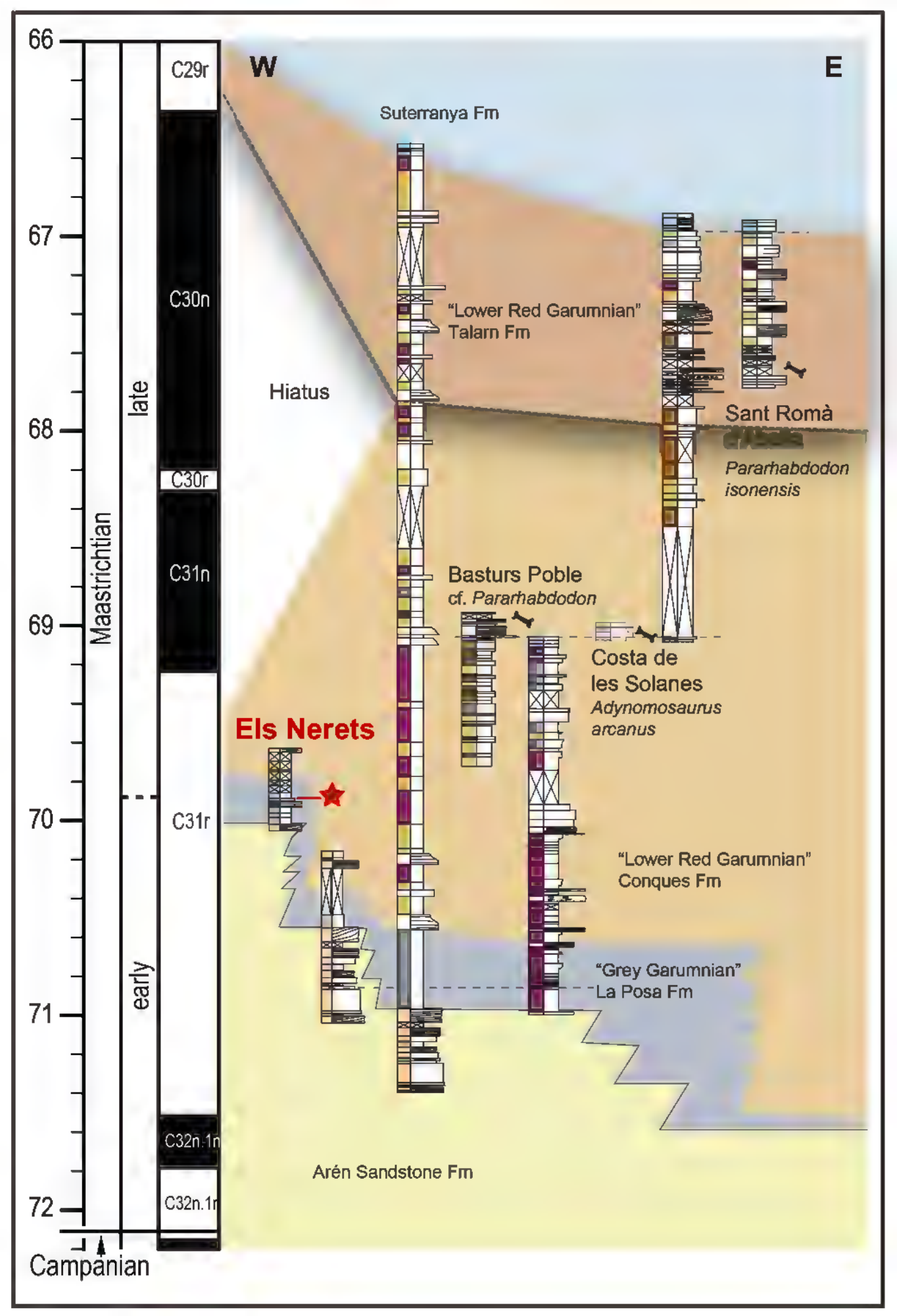
66
67
68
69
70
71
72
C29r
C30n
C30r
C31n
C31r
C32n.1n
C32n.1r
late
early
Maastrichtian
Campanian
W
E
Suterranya Fm
"Lower Red Garumnian"
Talarn Fm
Hiatus
Sant Romà
Pararhabdodon
isonensis
Basturs Poble
cf. Pararhabdodon
Costa de
les Solanes
Adynomosaurus
arcanus
Els Nerets
"Lower Red Garumnian"
Conques Fm
"Grey Garumnian"
La Posa Fm
Arén Sandstone Fm

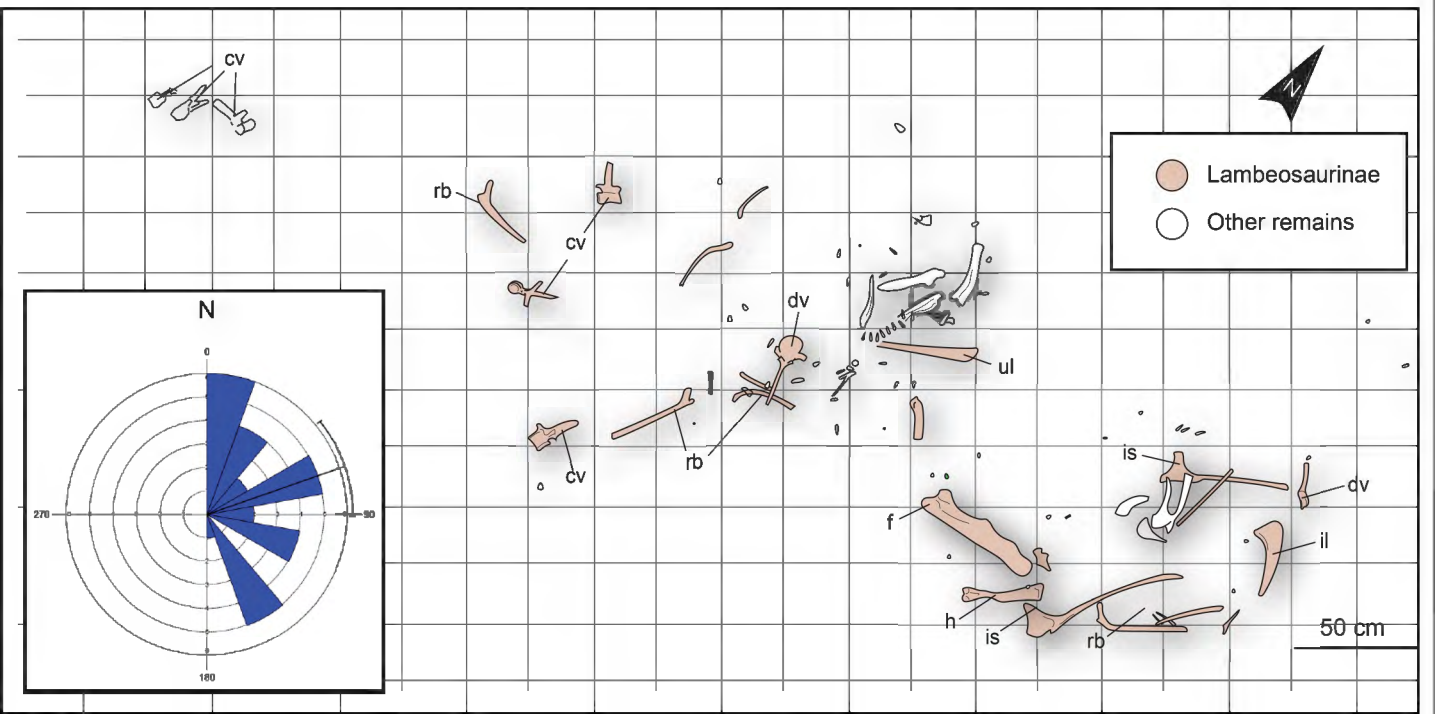
cv
rb
cv
dv
ul
cv
rb
N
0
90
180
270
Lambeosaurinae
Other remains
is
dv
f
il
h
is
rb
50 cm

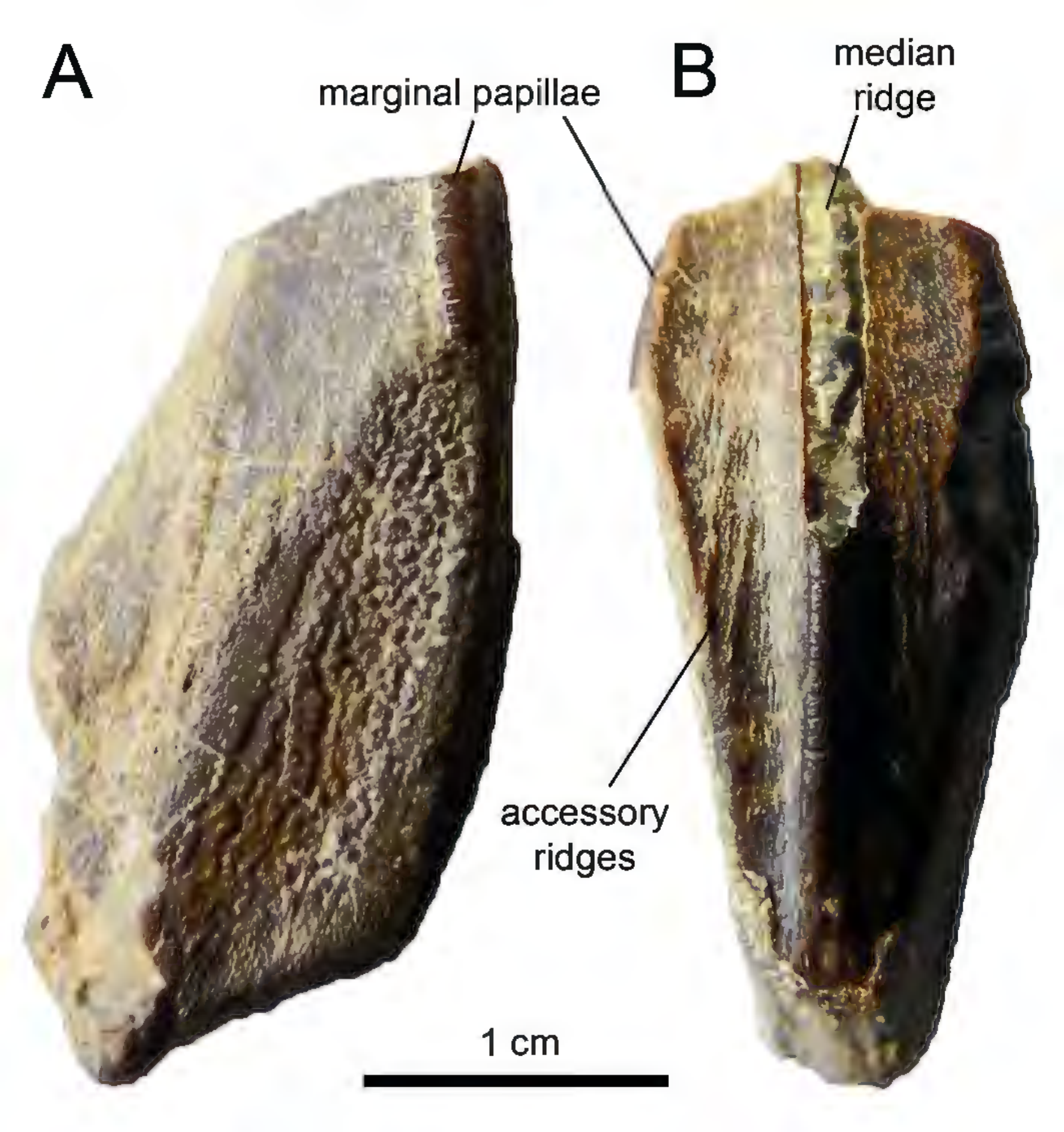
A
marginal papillae
B
median ridge
accessory ridges
1 cm

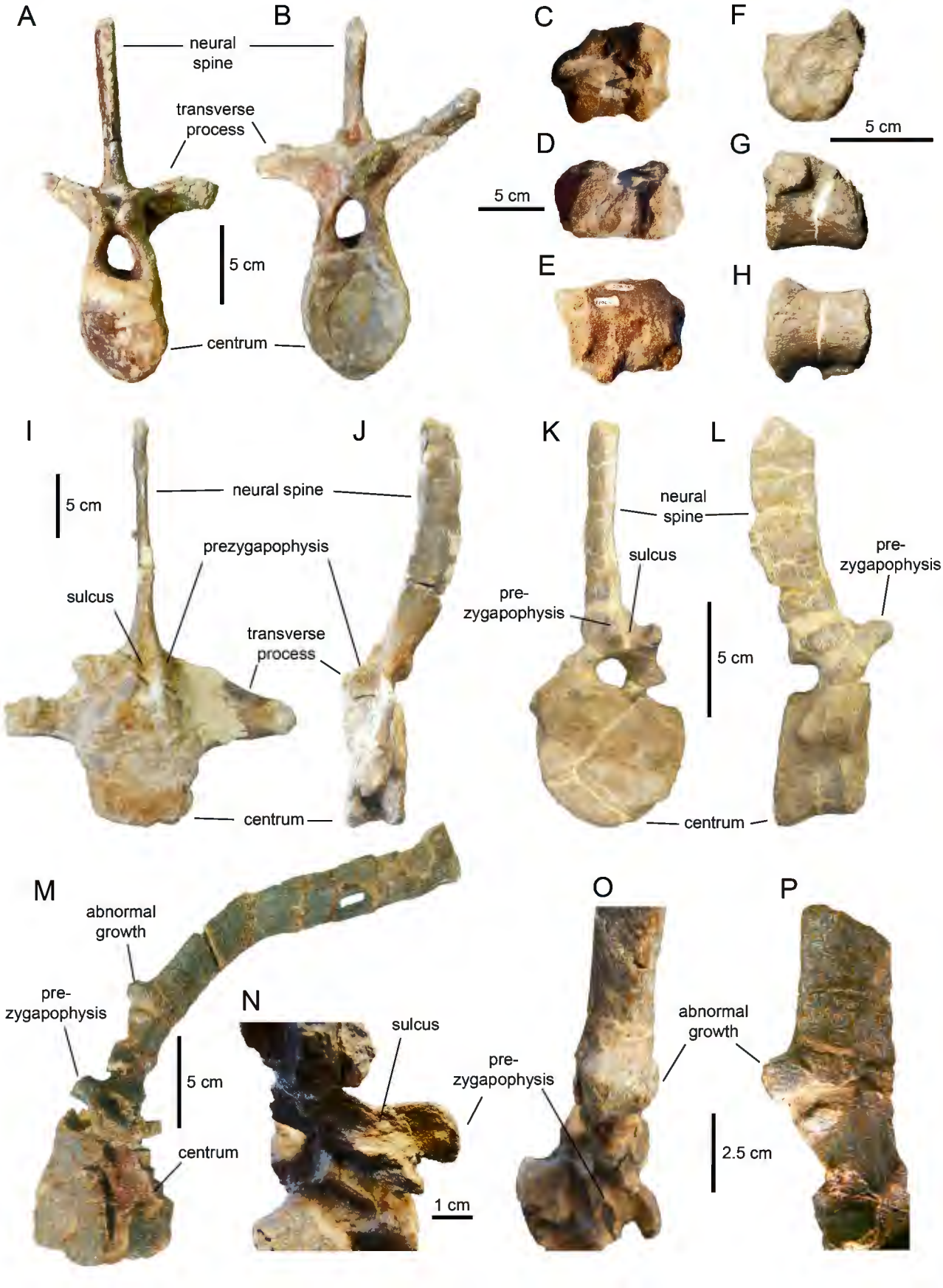
A
B
neural spine
transverse process
5 cm
centrum
C
D
5 cm
E
F
5 cm
G
H
I
J
5 cm
neural spine
prezygapophysis
sulcus
transverse process
centrum
K
L
neural spine
sulcus
pre-zygapophysis
5 cm
pre-zygapophysis
centrum
M
abnormal growth
pre-zygapophysis
5 cm
centrum
N
sulcus
pre-zygapophysis
1 cm
O
P
abnormal growth
2.5 cm

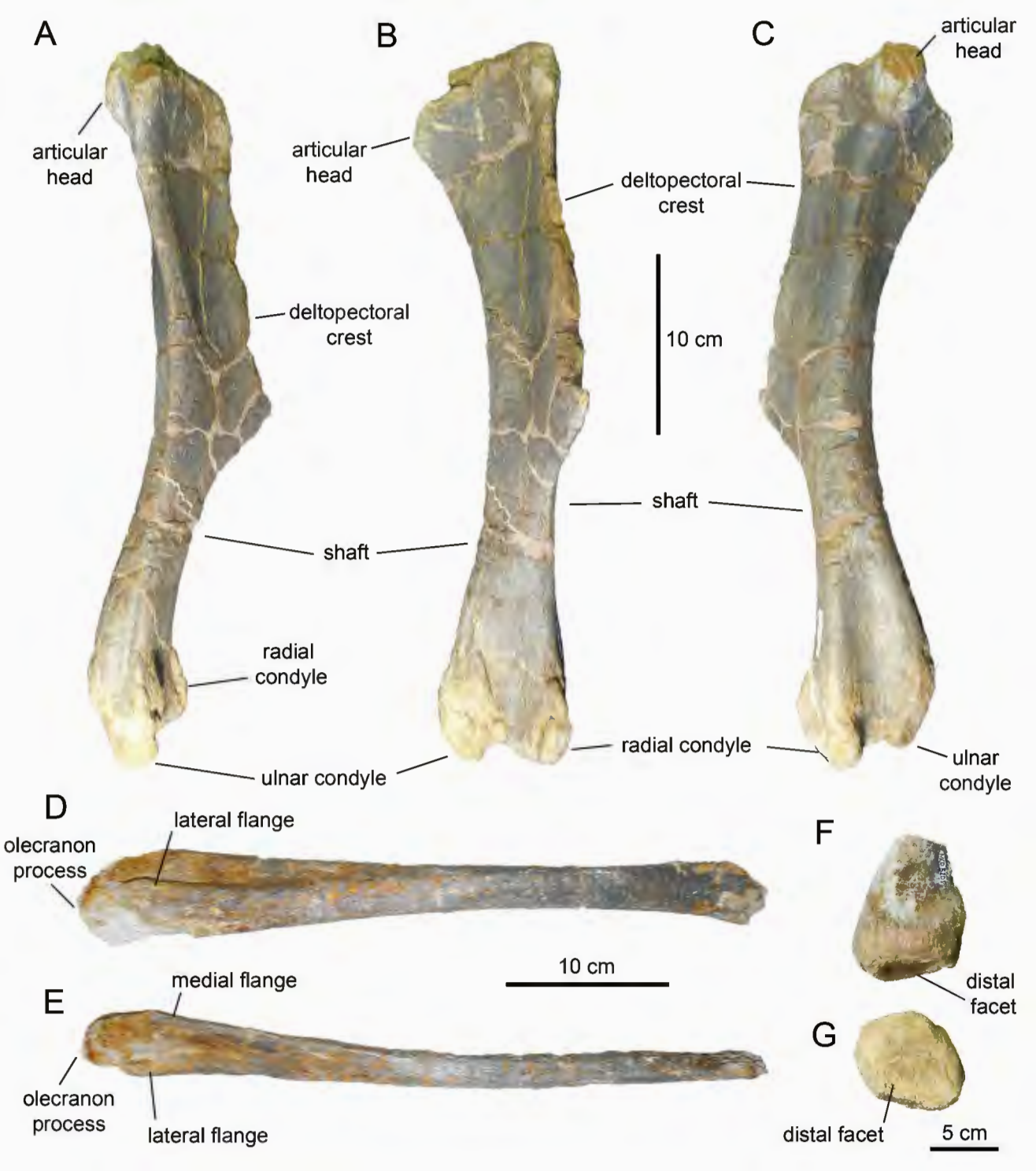
A
articular head
deltopectoral crest
shaft
radial condyle
ulnar condyle
B
articular head
deltopectoral crest
10 cm
shaft
radial condyle
C
articular head
ulnar condyle
D
olecranon process
lateral flange
10 cm
E
medial flange
olecranon process
lateral flange
F
distal facet
G
distal facet
5 cm

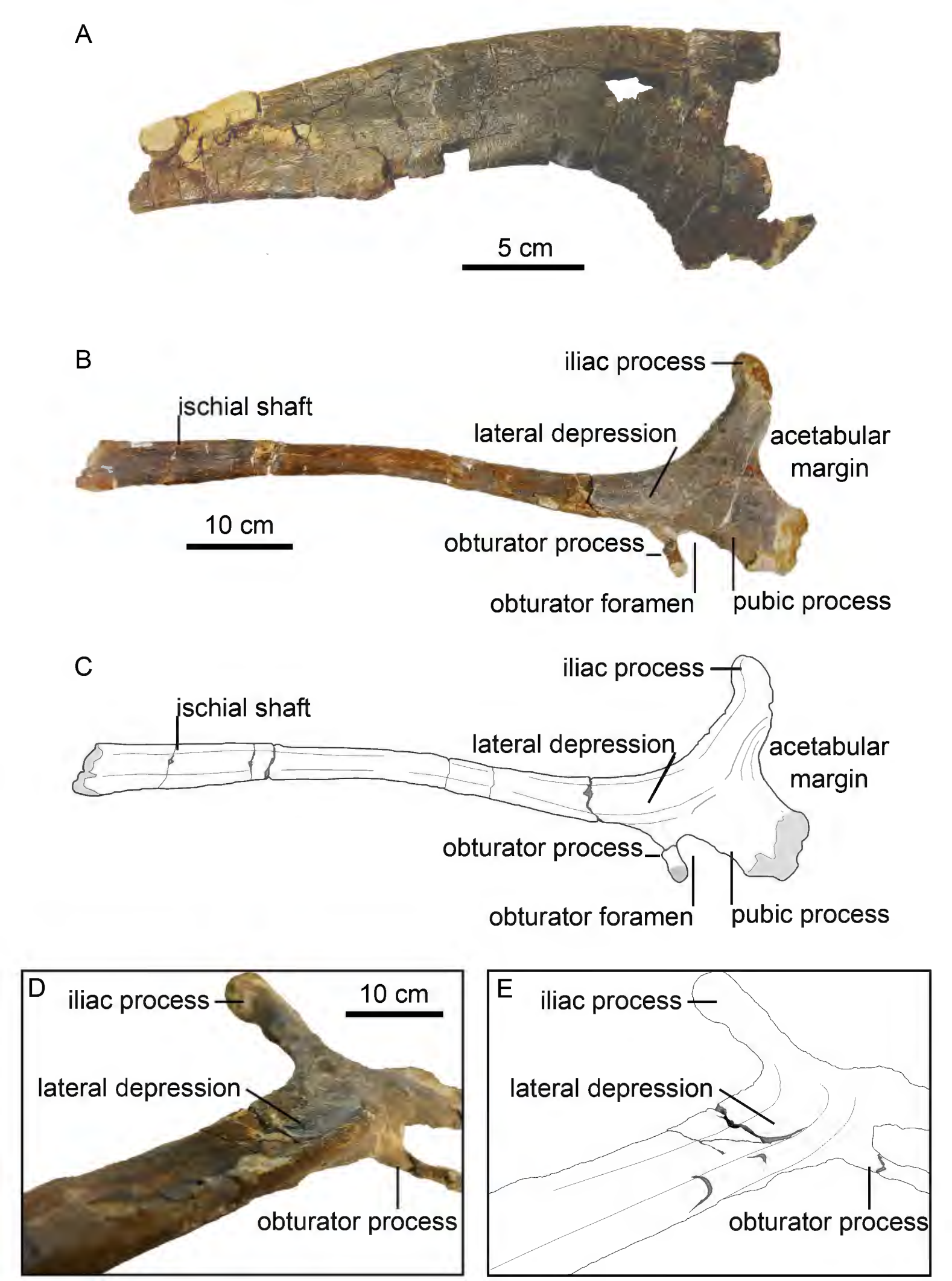
A
5 cm
B
iliac process
ischial shaft
lateral depression
acetabular margin
10 cm
obturator process
obturator foramen
pubic process
C
iliac process
ischial shaft
lateral depression
acetabular margin
obturator process
obturator foramen
pubic process
D
iliac process
10 cm
lateral depression
obturator process
E
iliac process
lateral depression
obturator process

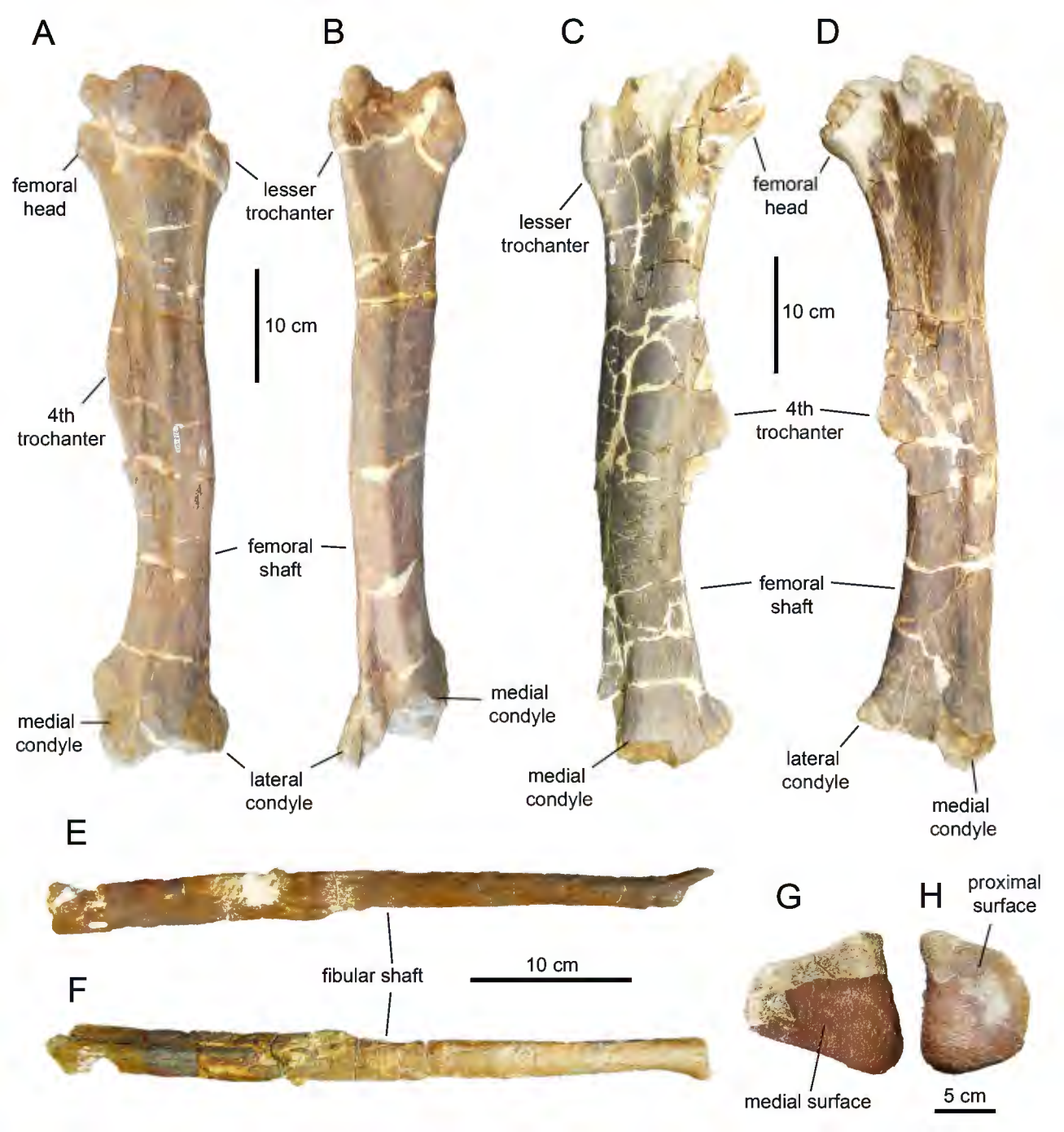
A
B
C
D
femoral head
lesser trochanter
10 cm
4th trochanter
femoral shaft
medial condyle
lateral condyle
lesser trochanter
femoral head
10 cm
4th trochanter
femoral shaft
medial condyle
lateral condyle
medial condyle
E
F
fibular shaft
10 cm
G
H
proximal surface
medial surface
5 cm

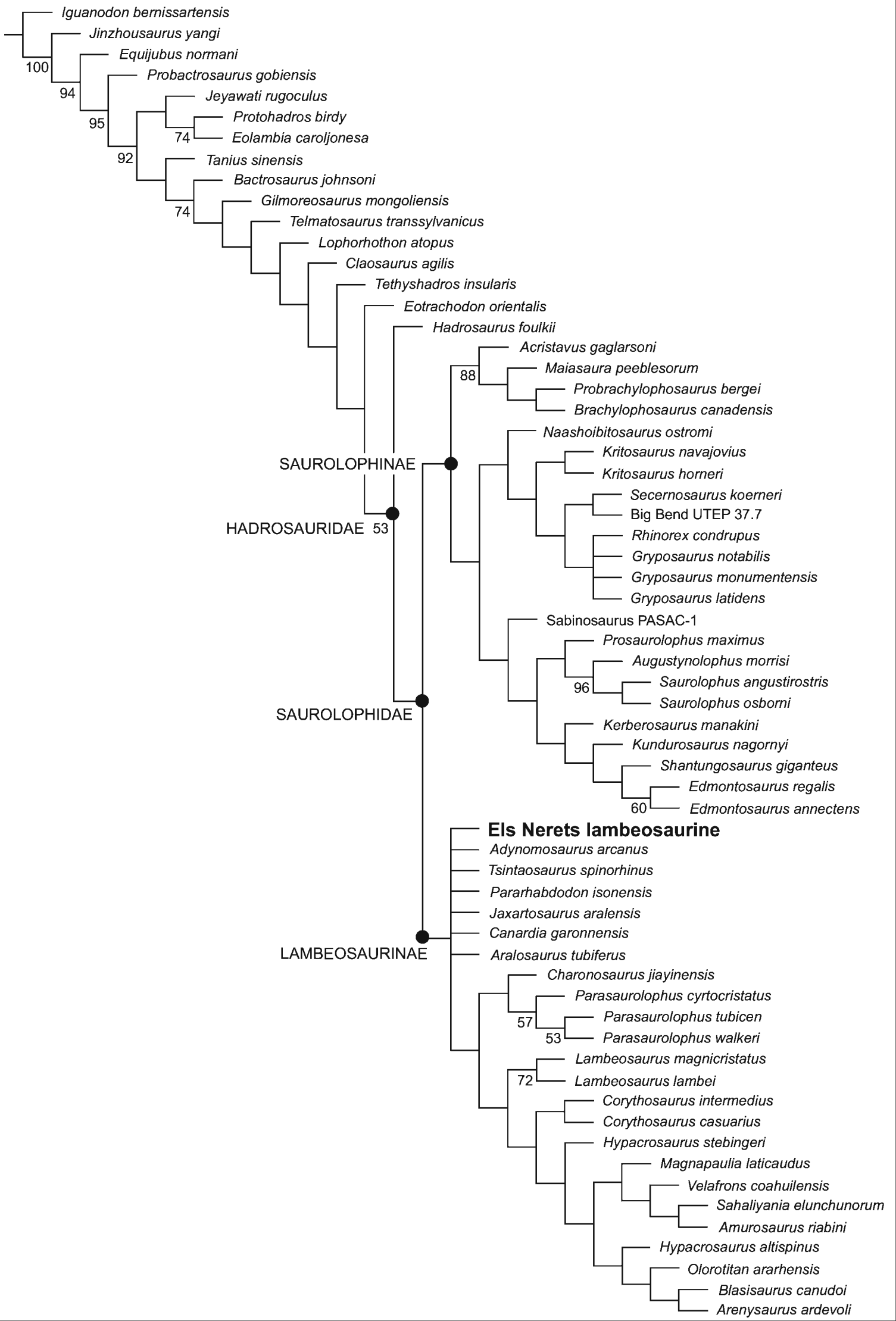
Iguanodon bernissartensis
Jinzhousaurus yangi
Equijubus normani
100
Probactrosaurus gobiensis
94
Jeyawati rugoculus
95
Protohadros birdy
74
Eolambia caroljonesa
92
Tanius sinensis
Bactrosaurus johnsoni
74
Gilmoreosaurus mongoliensis
Telmatosaurus transsylvanicus
Lophorhothon atopus
Claosaurus agilis
Tethyshadros insularis
Eotrachodon orientalis
Hadrosaurus foulkii
Acristavus gaglarsoni
88
Maiasaura peeblesorum
Probrachylophosaurus bergei
Brachylophosaurus canadensis
Naashoibitosaurus ostromi
SAUROLOPHINAE
Kritosaurus navajovius
Kritosaurus horneri
Secernosaurus koerneri
HADROSAURIDAE 53
Big Bend UTEP 37.7
Rhinorex condrupus
Gryposaurus notabilis
Gryposaurus monumentensis
Gryposaurus latidens
Sabinosaurus PASAC-1
Prosaurolophus maximus
Augustynolophus morrisi
96
Saurolophus angustirostris
Saurolophus osborni
SAUROLOPHIDAE
Kerberosaurus manakini
Kundurosaurus nagornyi
Shantungosaurus giganteus
Edmontosaurus regalis
60
Edmontosaurus annectens
Els Nerets lambeosaurine
Adynomosaurus arcanus
Tsintaosaurus spinorhinus
Pararhabdodon isonensis
Jaxartosaurus aralensis
Canardia garonnensis
LAMBEOSAURINAE
Aralosaurus tubiferus
Charonosaurus jiayinensis
Parasaurolophus cyrtocristatus
57
Parasaurolophus tubicen
53
Parasaurolophus walkeri
Lambeosaurus magnicristatus
72
Lambeosaurus lambei
Corythosaurus intermedius
Corythosaurus casuarius
Hypacrosaurus stebingeri
Magnapaulia laticaudus
Velafrons coahuilensis
Sahaliyania elunchunorum
Amurosaurus riabini
Hypacrosaurus altispinus
Olorotitan ararhensis
Blasisaurus canudoi
Arenysaurus ardevoli